Cookbook asymptotics for spiral and scroll waves in excitable media

Daniel Margerit and Dwight Barkley[a)]
Mathematics Institute, University of Warwick, Coventry CV4 7AL, United Kingdom

(Received 6 February 2002; accepted 29 May 2002; published 8 August 2002)

Algebraic formulas predicting the frequencies and shapes of waves in a reaction–diffusion model of excitable media are presented in the form of four recipes. The formulas themselves are based on a detailed asymptotic analysis (published elsewhere) of the model equations at leading order and first order in the asymptotic parameter. The importance of the first order contribution is stressed throughout, beginning with a discussion of the Fife limit, Fife scaling, and Fife regime. Recipes are given for spiral waves and detailed comparisons are presented between the asymptotic predictions and the solutions of the full reaction–diffusion equations. Recipes for twisted scroll waves with straight filaments are given and again comparisons are shown. The connection between the asymptotic results and filament dynamics is discussed, and one of the previously unknown coefficients in the theory of filament dynamics is evaluated in terms of its asymptotic expansion. © *2002 American Institute of Physics.* [DOI: 10.1063/1.1494875]

Propagating waves of excitation are frequently found in chemical media such as Belousov–Zhabontinskii reagent and in biological media such as nerve cells and cardiac muscle. In two space dimensions these waves commonly take the form of rotating spirals. In three dimensions these waves can take quite exotic forms, but commonly the underlying spatial structure is that of a scroll. The observation of these waves in an ever increasing number of situations presents a range of fundamental questions concerning their selection, dynamics, and biological function. The focus of this paper is the issue of pattern selection—specifically how results from asymptotic analyses of model reaction–diffusion equations lead to accurate predictions for the shape and rotation frequency of waves in homogeneous excitable media.

I. INTRODUCTION

Rotating spiral and scroll waves are a common occurrence in two- and three-dimensional excitable media.[1,2] One of the basic issues for such waves is the pattern selection problem: In a homogeneous medium free from defects, what selects the rotation frequency and the shape of the waves and how can these properties be predicted from underlying equations? This problem has been considered by a number of authors over the years.[3–20] Either directly or indirectly the approach is always to exploit the inherent scale separation in excitable media. The time scale of excitation is vastly shorter than that of recovery. As a result, the regions of rapid change in the medium are very small compared with typical length scales, e.g., the wavelength, of the pattern.

The most complete progress on pattern selection in excitable media has been made by addressing the free-boundary problem first proposed by Fife.[4,6,9,12,13,16,17,20] The medium is divided into appropriate regions and appropriate expansions are made in each region. Asymptotic matching is then used to reduce the problem of wave propagation to the motion of a free-boundary separating excited and quiescent (unexcited) regions of the medium. In this way the pattern selection problem becomes similar to a variety of other interfacial pattern formation problems such as solidification fronts and multiphase flow.[21]

Recently we reported preliminary results on the extension of the free-boundary approach beyond leading order in the small parameter.[20] As we shall show throughout this paper, the extension to next order in the small parameter provides accurate predictions in large parameter regions which have hitherto been unaccessible analytically. The purpose of this work is threefold: (1) to clarify terms and concepts which are not given precise meanings in the literature, in part because until the recent extension of asymptotics to first order, such precision has not been required; (2) to show, by means of simple algebraic recipes, how asymptotic results can be used in a variety of conditions; (3) to give a fairly comprehensive comparison, over a range of conditions, of the results of asymptotic predictions with full solutions of partial differential equations.

II. BACKGROUND

A. Model equations

We begin by considering a standard two-species reaction–diffusion model of excitable media:[22–24]

$$\partial u/\partial t_n = D_n \nabla_n^2 u + f(u,v)/\varepsilon_n, \tag{1a}$$

$$\partial v/\partial t_n = g(u,v). \tag{1b}$$

The parameter ε_n is small.

We shall consider the following specific functions modeling reaction kinetics:

$$f(u,v) = u(1-u)\left(u - \frac{v+b}{a}\right), \tag{2a}$$

a)Author to whom correspondence should be addressed. Electronic mail: barkley@maths.warwick.ac.uk

$$g(u,v)=u-v, \tag{2b}$$

where the parameters a and b control the excitability threshold and duration in the model. The function f has an N-shaped nullcline with two stable branches. It is not necessary that f be a cubic nonlinear function as in Eq. (2a), but this is the easiest case to consider. The function g is linear, and while this is also not required, it is the simplest case. For concreteness we shall consider only reaction kinetics (2) in this paper; however, the analysis applies equally to all similar models, such as the classical Fitzhugh–Nagumo equations. For $D_n=1$ the units in Eqs. (1) are those commonly used for this model.

Equations (1) are written in a ''laboratory'' or ''natural'' system of units (denoted by the subscript n). Equations coming from physiology might be written in such a form prior to any rescaling. The characteristic time scale of u is fast, owing to the factor $1/\varepsilon_n$ in Eq. (1a), while the characteristic time scale of v is order one. There is not a single best choice of units for the equations or even one choice for what might be considered appropriate ''laboratory'' units. Winfree,[25] for example, has considered a number of scalings for the reaction–diffusion equations, each corresponding to a particular choice of length and time units. For our purposes Eqs. (1) is a sufficient example. We need only one other particular scaling of the equations which we explain momentarily.

Consider the behavior of spiral-wave solutions of Eqs. (1) as the value of ε_n is reduced to zero. One finds that in the units in which Eqs. (1) are written, the spiral frequency ω_n diverges to infinity. This is shown in Fig. 1 for a typical set of parameter values. Simultaneously, it is found that the spiral wavelength goes to zero as $\varepsilon_n \to 0$ (not shown). However, there is freedom in the choice of length and time units in which to write the equations. In general, other choices will result in the frequency either diverging to infinity or else going to zero as epsilon goes to zero. Likewise, the wavelength will not remain finite and nonzero as ϵ_n goes to zero in general.

It was Fife[4] who first proposed the appropriate choice of units such as to give a *finite, nonzero* frequency and wavelength as ε goes to zero. The change of units is given in Table I. The small parameter ε_n is also rescaled for convenience. Reaction–diffusion equations (1) rewritten in these units become

$$\partial u/\partial t=\nabla^2 u+f(u,v)/\varepsilon^2, \tag{3a}$$

$$\partial v/\partial t=\varepsilon g(u,v). \tag{3b}$$

For a perturbation analysis in powers of ε it is normal to multiply through the first equation by ε^2. However, for numerical work it is better to consider the equations as given here. In addition, in this form ones see directly the difference with Eqs. (1).

In these equations, as in Eqs. (1), $\varepsilon=0$ is a singular parameter value and is not obtainable. However, unlike for Eqs. (1), spiral solutions to Eqs. (3) approach a sensible limit as ε goes to zero. See, for example, Fig. 1(c) showing the approach to a finite, nonzero frequency for spiral solutions to Eqs. (3).

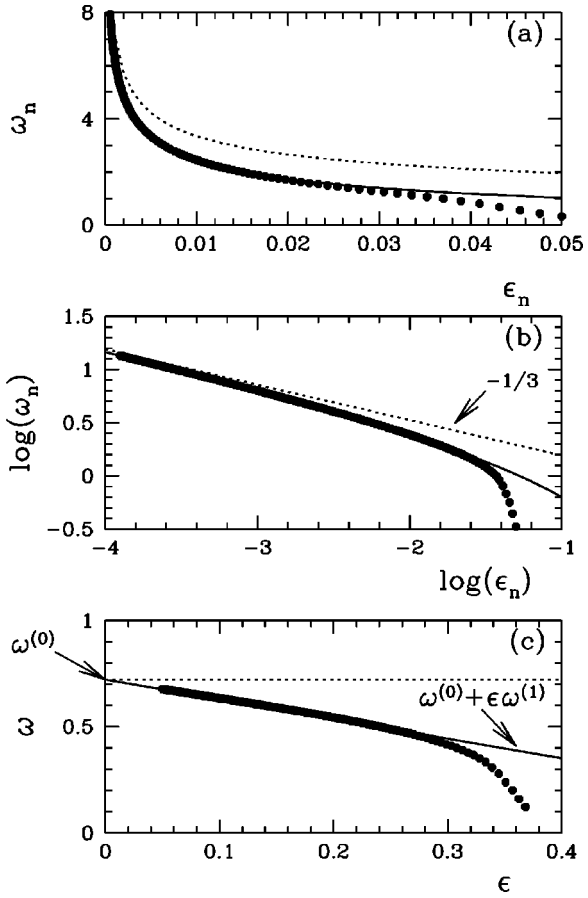

FIG. 1. Spiral frequency as a function of the small parameter in Eqs. (1) and (3) with $a=1.0$, $b=0.1$. Points are from numerical solutions to the reaction–diffusion equations. Dotted curves are the leading order, i.e., Fife-limit, asymptotic predictions. Solid curves are the asymptotic predictions including the first-order terms considered in this paper. (a) The divergence of the frequency, measured in ''laboratory'' or ''natural'' units, as the small parameter goes to zero. (b) Same as (a) except on a log–log scale. The leading-order asymptotic prediction is a straight line with slope $-1/3$. (c) Frequency in Fife units showing the finite limit obtained as $\varepsilon \to 0$. The leading-order plus first-order asymptotic prediction is the straight line.

B. Fife terms

It is necessary here to make precise certain terms which appear frequently in the literature, but which are not always given the precise meanings that we require. These terms are associated with the name Fife and involve the small epsilon behavior of solutions to the reaction–diffusion equations.

1. Fife limit

By the *Fife limit* we shall mean the limiting value of solutions of Eqs. (3) as $\varepsilon \to 0$. For example, the value $\omega^{(0)}$

TABLE I. Relationship between ''laboratory'' or ''natural'' units and Fife units. For completeness, frequency ω and wavelength λ are included.

Natural		Fife
$\varepsilon_n^{-1/6} D_n^{-1/2} x_n$	=	x
$\varepsilon_n^{-1/3} t_n$	=	t
$\varepsilon_n^{1/3}$	=	ε
$\varepsilon_n^{1/3} \omega_n$	=	ω
$\varepsilon_n^{-1/6} D_n^{-1/2} \lambda_n$	=	λ

illustrated in Fig. 1(c) is the spiral frequency in the Fife limit. The Fife limit corresponds to values at leading order in asymptotic expansions in the small parameter ε or ε_n.

2. Fife scaling and Fife units

In the literature the term *Fife scaling* is used to mean two closely related things. The first is the particular choice of units in Table I for which solutions are finite as ε goes to zero. For example, Eqs. (3) are said to be the reaction–diffusion equations written in the Fife scaling. To avoid confusion, we shall say Eqs. (3) are written in *Fife units*.

The other meaning of Fife scaling is as follows. Knowing the Fife limit of Eqs. (3), that is the leading-order asymptotic result in Fife units, it is possible to deduce the leading-order behavior of spirals in other systems of units. Consider, for example, the spiral frequency. In the natural units of Eqs. (1), we have directly by change of units that $\omega_n = \varepsilon_n^{-1/3}\omega^{(0)} + \cdots$ as $\varepsilon_n \to 0$. The leading-order scaling law for the frequency is thus $\omega_n \sim \varepsilon_n^{-1/3}$. Such a scaling law is often referred to as Fife scaling. It is implied immediately from the change of units in Table I and the fact that the spirals solutions of Eqs. (3) have a finite (Fife) limit as $\varepsilon \to 0$.

3. Fife regime

Finally we define the *Fife regime* as the range of epsilon for which the Fife limit is a useful approximation. This is a matter of opinion and will depend on model parameters in general.

C. Discussion

Over the years there has been considerable interest in the asymptotic analysis of spiral waves at leading order in epsilon (e.g., Refs. 6, 8, 9, 12, 13, and 16–19). These analyses give the Fife limit and the associated Fife scaling, for example, the relationship $\omega_n \sim \varepsilon_n^{-1/3}$.

Attempts have been made to verify this scaling through direct time-dependent numerical simulations of the reaction–diffusion equations.[12,25] Typically such verifications have been based on log–log plots such as shown in Fig. 1(b). Figure 1, which is an expanded presentation of the data first presented in Ref. 20, is the most complete verification of the Fife limit and associated Fife scaling to date. It covers a substantial range of epsilon down to quite small values. The solutions to the reaction–diffusion equations have been computed using Newton's method rather than by time-dependent simulations.[26,27]

The first thing to note about Fig. 1 is that working directly in Fife units is the best approach to understanding the behavior of spiral waves at small ε. This is true in large part because quantities have simple whole-power expansions in ε, e.g., $\omega = \omega^{(0)} + \varepsilon\omega^{(1)} + \cdots$. Working in units other than the Fife units tends to obscure the behavior as epsilon goes to zero and analyses based on log–log plots are not optimal. For example, the existence of a finite Fife limit is well supported by the data for only $\varepsilon > 0.15$ in Fig. 1(c), whereas the existence of Fife scaling (slope $-1/3$) in Fig. 1(b) is not well supported by the equivalent range, $\log(\varepsilon_n) > -2.5$. Surprisingly, despite the large interest in the Fife scaling, results are almost nowhere reported directly in Fife units.

Another important feature seen in Fig. 1 is that the Fife limit itself does not provide an accurate quantitative prediction of wave properties. That is, the Fife regime is not very large. (The exact size will be model and parameter dependent and may be larger in some cases.) Frequencies and other quantities are of the correct magnitude, but otherwise are not quantitatively accurate. However, as the solid curves in Fig. 1 show, an asymptotic expansion to next order (order ε in Fife units) is accurate over a considerable range in epsilon. At the upper end of the range epsilon shown in Fig. 1, where the spiral frequency begin to decrease rapidly, the medium is only weakly excitable. The frequency falls to zero and beyond this point the medium does not support spiral waves (see Refs. 15, 19, 25, 28, and 29).

Throughout the bulk of the paper we shall work exclusively in Fife units and consider asymptotic expansions to first order in ε. At the end we return to the units of Eqs. (1).

III. SPIRAL RECIPES

The goal of the selection problem is to find the rotation frequency and shape of spiral waves as a function of the parameters appearing in Eqs. (3), or equivalently Eqs. (1). In practice this is accomplished via matched-asymptotic expansions. In this section we review equations obtained elsewhere[6,9,12,20] using such techniques. We do not concern ourselves with the details of the derivations. Instead we focus on the key ideas which are important for *using* the asymptotic results. In particular, we provide procedures for obtaining approximations to the spiral shape and frequency without further need for solving any differential equations.

A. Ingredients

We consider spirals which are rigidly rotating at a constant frequency ω. We work with polar coordinates (r,φ) based on the center of spiral rotation and consider solutions in a corotating frame of reference in which the spiral is a steady state. The spiral shape is described by two curves, a wave front and a wave back given by the functions $\Phi^+(r)$ and $\Phi^-(r)$, respectively. Points on the wave back are represented parametrically by $(r, \varphi = \Phi^-(r))$ and similarly for the wave front. Together, the two curves divide the domain into the excited and quiescent regions.

The wave front and wave back actually represent thin interfaces in which the fast u variable makes a rapid change between the quiescent value $u = 0$ and the excited value $u = 1$. Only on the outer asymptotic scale are the interfaces one-dimensional curves. The transition between $u = 0$ and $u = 1$ must be resolved on an inner asymptotic scale. Where the wave front and wave back come together at the center of rotation there is a small asymptotic region, the core, which must be resolved on an inner scale.

In the asymptotic derivation, the different regions are written in appropriate coordinates, solutions are sought in powers of ε, and inner and outer solutions are matched to obtain a complete asymptotic solution. Our only concern here is the final results on the outer scale. In particular, our

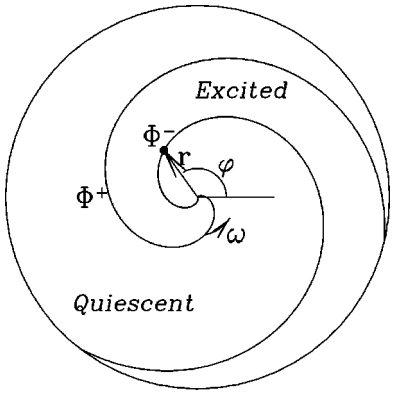

FIG. 2. Sketch of the spiral geometry and coordinates. The spiral is described by the two interfaces: a wave front $\Phi^+(r)$ and a wave back $\Phi^-(r)$. These interfaces separate the medium into excited and quiescent regions. The spiral rotates with angular frequency ω. Positive ω corresponds to counter-clockwise rotation.

interest is in the rotation frequency and interface shape represented by their ε expansions

$$\omega=\omega^{(0)}+\varepsilon\omega^{(1)}+\cdots, \tag{4}$$

$$\Phi^{\pm}(r)=\Phi^{(0)\pm}(r)+\varepsilon\Phi^{(1)\pm}(r)+\cdots. \tag{5}$$

We consider the results for the first two orders: leading order, ε^0, which is equivalent to the Fife limit, and first order, ε^1.

We consider only the chirality shown in Fig. 2, because it corresponds naturally to a positive rotation frequency. Spirals with the opposite chirality can be obtained trivially for those found below.

B. Leading-order recipe

At leading order solutions can be found for which the wave front and wave back are identical in shape with a constant angular separation between the two (independent of r).[9,12,20] For example, the wave front and wave back drawn in Fig. 2 are of identical shape.

The angular separation between the front and back is given by

$$\Delta\Phi^{(0)}\equiv\Phi^{(0)+}-\Phi^{(0)-}=2\pi v^s, \tag{6}$$

where v^s is the stall concentration of v: the value of v at a planar interface such that the velocity of the interface is zero. The value depends on the particular model kinetics and parameter values, and is given below for Eqs. (2).

The interface shape and frequency obey a single universal equation:

$$\frac{d\Psi^{(0)}}{d\tilde{r}}+\frac{\Psi^{(0)}(1+\Psi^{(0)2})}{\tilde{r}}=\tilde{r}(1+\Psi^{(0)2})-B(1+\Psi^{(0)2})^{3/2}, \tag{7}$$

where $\Psi^{(0)}(\tilde{r})$ is the universal shape function describing both interfaces and $\tilde{r}$ is the universal radial coordinate. These are defined by

$$\Psi^{(0)}(\tilde{r})\equiv\tilde{r}\,d\Phi^{(0)+}/d\tilde{r}=\tilde{r}\,d\Phi^{(0)-}/d\tilde{r}, \tag{8}$$

$$\tilde{r}\equiv\sqrt{\omega^{(0)}}r. \tag{9}$$

The boundary condition at $\tilde{r}=0$ for Eq. (7) is

$$\Psi^{(0)}(\tilde{r}=0)=0, \tag{10}$$

while the physically relevant large-$\tilde{r}$ behavior of $\Psi^{(0)}$, obtained by expanding Eq. (7) in inverse powers of $\tilde{r}$, is

$$\Psi^{(0)}(\tilde{r}\to\infty)=-\frac{\tilde{r}}{B}-\frac{1}{B^2}+\left(\frac{B}{2}-\frac{1}{B^3}\right)\frac{1}{\tilde{r}}+O\left(\frac{1}{\tilde{r}^2}\right). \tag{11}$$

This expression is particularly important because it captures the essential shape of the spiral away from the center.

Finally, the eigenvalue B appearing in Eq. (7) is related to the leading order frequency $\omega^{(0)}$ via

$$B=(\mu/\omega^{(0)})^{3/2}, \tag{12}$$

where μ depends on the particular model kinetics and parameters. For Eqs. (2) we have

$$v^s=a/2-b, \tag{13}$$

$$\mu^{3/2}=\sqrt{2}\pi v^s(1-v^s)/a. \tag{14}$$

1. Comments

Equation (7) is universal because it is independent of details of the reaction kinetics and model parameters for a large class of models.[6,9,12] The model and parameter specific details are contained in the relationship between the eigenvalue B and frequency $\omega^{(0)}$, and in the relationship between the universal coordinate $\tilde{r}$ and the radial coordinate r. It should be realized that time and space scalings have already been accounted in Eqs. (3) from which Eq. (7) is derived; the further multiplication of r by the square root of a frequency (a pure number) is simply how model-dependent details are accounted for in a universal way.

The selection mechanism for spiral patterns at leading order is as follows. The universal equation is a nonlinear eigenvalue problem. It has a unique solution with the required boundary condition at zero, Eq. (10), and the correct behavior at infinity, Eq. (11), only for a specific value of B, the selected value. For any other value of B the solution $\Psi^{(0)}(\tilde{r})$ changes sign and goes to infinity as $\Psi^{(0)}(\tilde{r}\to\infty)=+\tilde{r}/B$, cf. Eq. (11), possibly by going through a singularity at finite $\tilde{r}$. The result is the selected value of B,[6,9,12]

$$B=1.7383\ldots, \tag{15}$$

and the universal shape function $\Psi^{(0)}(\tilde{r})$.

From the selected value of B, the selected leading order frequency $\omega^{(0)}$ is given via Eq. (12). The selected spiral shape $\Phi^{(0)}$ comes from the solution $\Psi^{(0)}$ itself. For most purposes all that is required is the value of B and the large-r limit (11). From these the leading order shape can be found to a good approximation.

2. Recipe 1

The following is a recipe for obtaining leading-order approximations to spiral waves in Eqs. (3) with kinetics given by Eqs. (2).

Use Eqs. (13) and (14) find v^s and μ for desired model parameters a and b. Then from the value of B in Eq. (15) obtain the leading-order frequency and spiral shape via

$$\omega^{(0)} = \mu/B^{2/3}, \tag{16a}$$

$$\Phi^{(0)+}(r) = \Phi_0 - k^{(0)} r - \frac{1}{B^2}\ln r\,, \tag{16b}$$

$$\Phi^{(0)-}(r) = \Phi^{(0)+}(r) - 2\pi v^s, \tag{16c}$$

where

$$k^{(0)} = \frac{\sqrt{\omega^{(0)}}}{B}, \tag{16d}$$

and where Φ_0 is a constant of integration which sets the phase of the spiral. Note that by our convention (Fig. 2), the spiral frequency is positive. We also define $k^{(0)}$ to be positive. The fact that $d\Phi^+/dr$ is negative for spirals with positive frequency ω is accounted for with the minus signs in Eq. (16b). Comparisons with numerical solutions of Eqs. (3) are given in Sec. IV.

C. First-order recipe

We turn to the asymptotics at order ε. The result of the matched asymptotic analysis[20] is that at order ε the front and back interfaces again have the same shape. The contribution to the angular separation at first order is zero,

$$\Delta\Phi^{(1)} = \Phi^{(1)+} - \Phi^{(1)-} = 0. \tag{17}$$

The universal equation for the first-order contribution to the interface shape and frequency is

$$\frac{d\Psi^{(1)}}{d\tilde{r}} + l(\tilde{r})\Psi^{(1)} = Dm_1(\tilde{r}) + m_2(\tilde{r}), \tag{18}$$

where the universal shape function at first order is defined by

$$\Psi^{(1)}(\tilde{r}) \equiv a\omega^{(0)}\tilde{r}\, d\Phi^{(1)+}/d\tilde{r} = a\omega^{(0)}\tilde{r}\, d\Phi^{(1)-}/d\tilde{r}. \tag{19}$$

The universal coordinate $\tilde{r}$ is defined as before [Eq. (9)].

The functions appearing in Eq. (18) depend on the leading-order shape $\Psi^{(0)}(\tilde{r})$ and are given by

$$l(\tilde{r}) = \frac{1}{\tilde{r}} + \tilde{r}\Psi^{(0)} + 3\Psi^{(0)}\left[\frac{\Psi^{(0)}}{\tilde{r}} - \tilde{r} + B\sqrt{1+\Psi^{(0)2}}\right],$$

$$m_1(\tilde{r}) = \tilde{r}(1+\Psi^{(0)2}) + B(1+\Psi^{(0)2})^{3/2},$$

$$m_2(\tilde{r}) = \frac{5}{3}\frac{(1+\Psi^{(0)2})^2}{\tilde{r}}.$$

The universal equation at first order is linear in the shape function. The solution is found by first finding the solution $\Psi_h^{(1)}$ to the homogeneous problem. The solution is

$$\Psi_h^{(1)} = \frac{1}{\tilde{r}}(1+\Psi^{(0)2})^{3/2}\exp\left(-\int_0^{\tilde{r}}\rho\Psi^{(0)}(\rho)d\rho\right). \tag{20}$$

Then the solution of Eq. (18) which is finite at the origin is given by

$$\Psi^{(1)}(\tilde{r}) = \Psi_h^{(1)}(\tilde{r})\int_0^{\tilde{r}}\frac{Dm_1(\rho)+m_2(\rho)}{\Psi_h^{(1)}(\rho)}d\rho. \tag{21}$$

Solutions (20) and (21) can easily be verified by direct substitution.

One may obtain the shape away from the core by using the large-$\tilde{r}$ behavior of $\Psi^{(1)}$ from Eq. (18),

$$\Psi^{(1)}(\tilde{r}\to\infty) = -\frac{6DB^2+5}{3B^3}\tilde{r} - \frac{3DB^2+5}{B^4} + O\left(\frac{1}{\tilde{r}}\right). \tag{22}$$

Finally, the eigenvalue D is proportional to the first-order frequency $\omega^{(1)}$. This proportionality is model dependent. For Eqs. (2) we have

$$D = a\omega^{(1)}. \tag{23}$$

1. Comments

The selection mechanism of the shape and frequency at first order is different from the selection at leading order. At first order the selection is as follows. Because $\Psi^{(0)}$ is negative, the exponential in Eq. (20) is positive, and hence the homogeneous solution diverges exponentially as $\tilde{r}\to\infty$. Hence $\Psi^{(1)}(\tilde{r})$ from Eq. (21) will also diverge exponentially unless

$$\int_0^{\tilde{r}}\frac{Dm_1(\rho)+m_2(\rho)}{\Psi_h^{(1)}(\rho)}d\rho \to 0 \quad \text{as} \quad \tilde{r}\to\infty. \tag{24}$$

This selects the value of D. The selected value can be written

$$D = -\frac{c_2}{c_1},$$

where

$$c_i = \int_0^{\infty}[m_i(\rho)/\Psi_h^{(1)}(\rho)]d\rho.$$

Given the value of D, the shape function $\Psi^{(1)}(\tilde{r})$ is found by the integrals in Eqs. (20) and (21). In practice all the integrals must be computed numerically (see Appendix A). One finds the value of D to be

$$D = -0.9261\ldots. \tag{25}$$

2. Recipe 2

Here we give a recipe for obtaining leading-plus-first-order approximations to spiral waves in Eqs. (3) with kinetics given by Eqs. (2).

First use Recipe 1 to obtain $\omega^{(0)}$ and $\Phi^{(0)\pm}$. Then calculate

$$\omega^{(1)} = D/a, \tag{26a}$$

$$\Phi^{(1)+}(r) = -k^{(1)}r, \tag{26b}$$

where

$$k^{(1)} = \frac{6DB^2+5}{3aB^3\sqrt{\omega^{(0)}}}. \tag{26c}$$

Then

$$\omega = \omega^{(0)} + \varepsilon \omega^{(1)}, \tag{27a}$$

$$\Phi^{+}(r) = \Phi^{(0)+}(r) + \varepsilon \Phi^{(1)+}(r), \tag{27b}$$

$$\Phi^{-}(r) = \Phi^{+}(r) - 2\pi v^{s}. \tag{27c}$$

Note that we have kept the same sign conventions as in Recipe 1 (e.g., positive ω corresponds to counter-clockwise rotation). However, both $\omega^{(1)}$ and $k^{(1)}$ have negative values.

Equations (27) give the spiral frequency and shape as a function of all three parameters a, b, and ε appearing in the reaction–diffusion equations.

IV. RESULTS: SPIRAL WAVES

In this section we present various comparisons of the asymptotic results and full solutions of reaction–diffusion equations (3) with kinetic terms (2).

A. Frequency comparison

We begin by considering the spiral rotation frequency. Because this is a simple scalar quantity, it is possible to show a rather comprehensive comparison between the asymptotic predictions and the actual frequencies obtained from the reaction–diffusion equations. In Fig. 3 we show frequency contours in the $a-b$ parameter plane for three values of ε. For each ε, five contours are selected decreasing from the largest spiral frequency at that value of ε. Similar frequency landscapes have been studied by Winfree.[25]

As expected, one sees that for small ε ($\varepsilon = 0.1$) the agreement between asymptotics and full numerical solutions is very good. See also Fig. 1(c). At moderate ε ($\varepsilon = 0.2$) the agreement is still reasonable. In quantitative terms, the asymptotics predicts the true frequencies to within about 10% for the frequencies whose contours are shown. Even at $\varepsilon = 0.271\,44$, which is quite a large value, the asymptotics captures the spirals which have large frequencies. The value $\varepsilon = 0.271\,44$ corresponds to $\varepsilon_n \simeq 0.02$, a value used in numerous previous publications.

For contrast, we show in Fig. 4 a comparison between the leading order frequency $\omega^{(0)}$ and full reaction–diffusion results at $\varepsilon = 0.2$, the same as in Fig. 3(b). The importance of the first-order correction is evident. Note that the effect of the first-order correction is to reduce the value of ω since $\omega^{(1)} < 0$. This can also be seen in Fig. 1.

The parameter range covered in Fig. 3 encompasses most of the excitable region in which spiral waves exist in Eqs. (3). There is a region of parameter space in which spiral waves do not exist owing to the inability of the medium to support waves.[15,19,25,28,29] This is known as propagation failure. This region is in the upper left part of the $a-b$ parameter plane and its size increases with increasing ε. On approaching this region the medium becomes only weakly excitable and the spiral rotation frequency falls to zero; the rotation period goes to infinity. This effect is seen in Fig. 1 as ε is increased for fixed a and b. As the frequency becomes small it is difficult to compute spiral solutions of the reaction–diffusion equations by our methods because spirals rotate about very large cores (hence the large rotation period), and very large domains are required. As is clear from Figs. 1 and 3, our asymptotic results are not predictive for weakly excitable media.

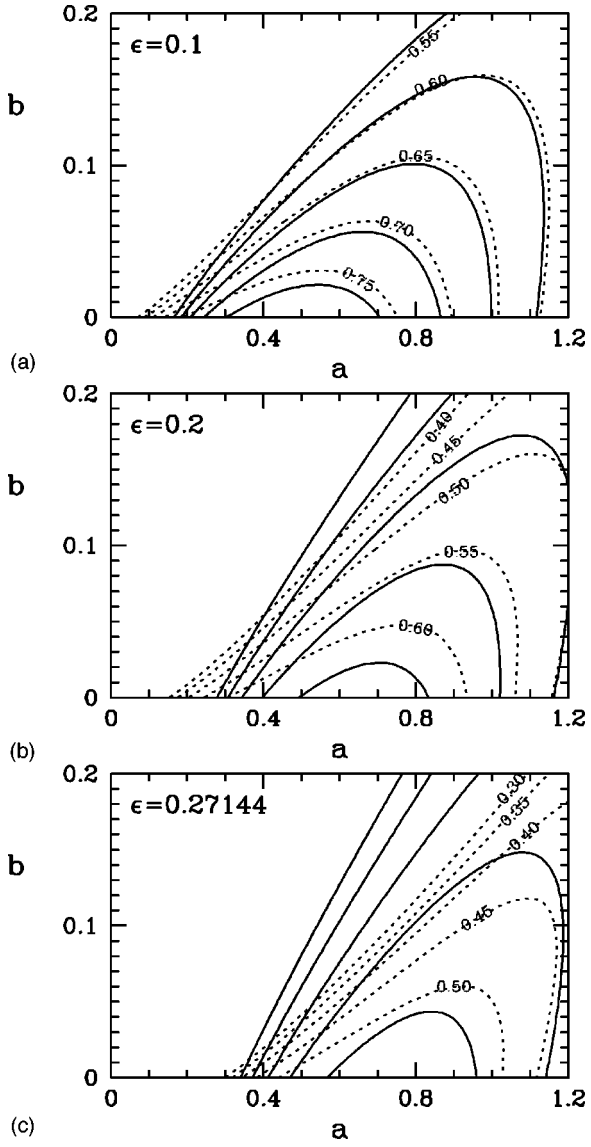

FIG. 3. Comparison of frequency ω from asymptotics at first order (solid) and full solutions of reaction–diffusion equations (dashed) for three values of ε. Frequency contours are shown in the $a-b$ parameter plane. The contour levels plotted vary with ε, but at each ε the contour levels for the reaction–diffusion equations (labeled) are the same as for the asymptotics (not labeled).

B. Shape comparison

We now consider how the spiral shapes obtained from asymptotics compare with the spirals solutions of the full reaction–diffusion equations. There are two distinct comparisons to be made here. First, the spiral shapes associated with solutions of universal equations, Eqs. (7) and (18), are compared to the spiral shapes that come from using large-r approximations to these solutions, Eqs. (11) and (22). The large-r approximations are used in our asymptotic recipes so it is important to assess the validity of these approximations. Then, we compare the shapes given by our recipes to spiral solutions of Eqs. (3).

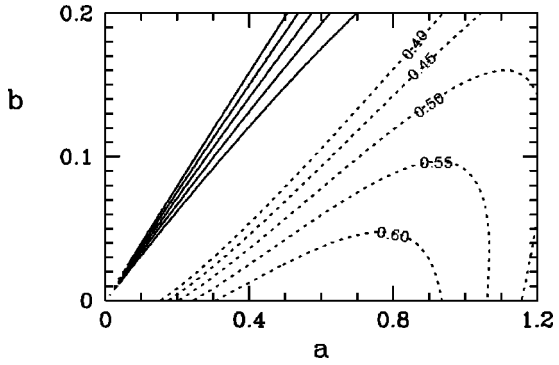

FIG. 4. Comparison of frequency ω from leading-order asymptotics (solid) and full solutions of reaction–diffusion equations (dashed) for $\varepsilon=0.2$. The frequency contour levels for the reaction–diffusion equations (labeled) are the same as for the asymptotics (not labeled).

Figures 5 and 6 show the first comparison. The universal equations are solved to obtain $\Phi^{(0)}(r)$ and $\Phi^{(1)}(r)$ for the specific parameters shown in the figures. Also plotted are the approximations to $\Phi^{(0)}(r)$ and $\Phi^{(1)}(r)$ obtained from Eqs. (11) and (22). For these approximations, we show the effect of including different numbers of terms, including in each case the effect of one more term than we keep in our recipes.

Consider first the leading-order case. The short-dashed curve is the Archimedean approximation $\Phi^{(0)}(r)=-k^{(0)}r$ where $k^{(0)}$ is the far-field pitch or wave number of the spiral. It is evident from Fig. 5 that while this single term does capture the large-r shape of the universal solution, this approximation is not very good at small and intermediate values of r. The long-dashed curve is the approximation $\Phi^{(0)}(r)=-k^{(0)}r-1/B^2\ln r$, which we use in our recipe. This approximation is almost indistinguishable from the solid curve on the scale of Fig. 5. Some deviation from the solid curve can be seen in the enlargement of Fig. 6. Note that the solution is plotted from small r ($r=0.1$) and yet the divergence due to the logarithmic term has not made itself felt. Finally we show with a dashed–dotted curve the approximation obtained including the next term from Eq. (11): $\Phi^{(0)}(r)=-k^{(0)}r-1/B^2\ln r-(B/2-1/B^3)/(\sqrt{\omega^{(0)}}r)$. On the scale of Fig. 5 there is no effect of including this term. On the scale of Fig. 6 it can be seen that there is a range in r for which the term does produce a better approximation to the exact solution. However, this improvement is modest and is outweighed by the $1/r$ divergence as $r\to 0$. For this reason and with a view to keep the recipes simple, we use a two-term approximation to $\Phi^{(0)}(r)$ in Recipe 1.

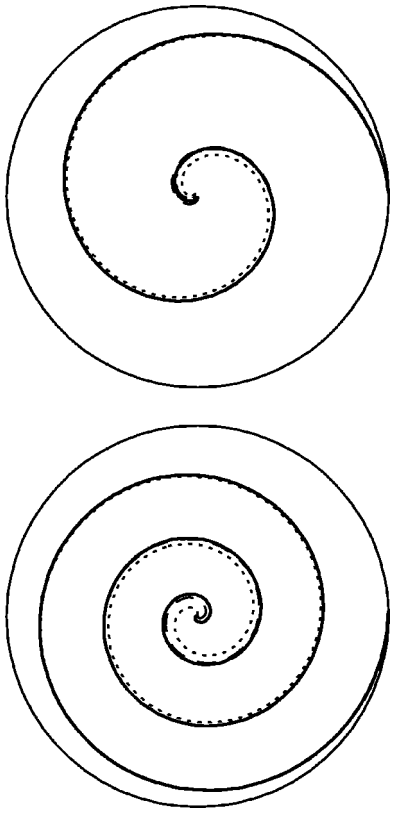

FIG. 5. Leading order spiral $\Phi^{(0)}(r)$ (top) and first-order correction $\Phi^{(1)}(r)$ (bottom) from asymptotic equations. Spirals from numerical solutions of the universal equations are shown as solid. Other curves show approximations (see text). Parameters $a=1.0$, $b=0.1$. Radius$=20$.

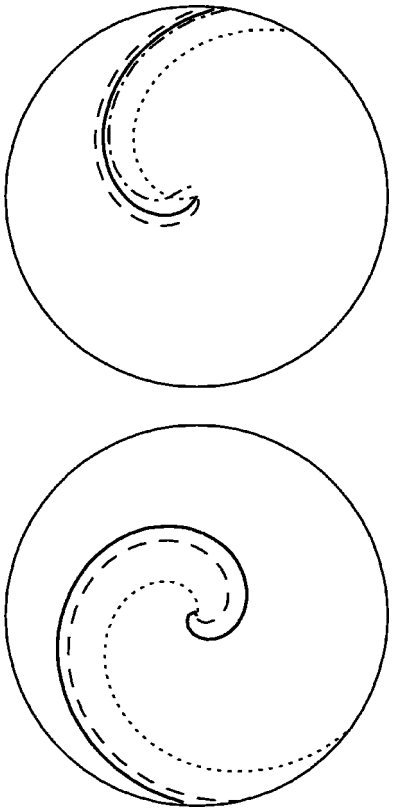

FIG. 6. Same as Fig. 5 except the domain radius is 5.

Now consider the first-order case. The short-dashed curve is the Archimedean approximation, this time $\Phi^{(1)}(r)=-k^{(1)}r$. Again this approximation is very good at large r but deviates from the solution of the universal solution at moderate and small values of r. We show as a long-dashed curve the approximation $\Phi^{(1)}(r)$ including the logarithmic term coming from Eq. (22). Clearly this term is useful for obtaining a good approximation to $\Phi^{(1)}(r)$. However, unlike for the leading-order solution, the first-order shape $\Phi^{(1)}$ is multiplied by ε in Eq. (27b) and so in fact the contribution from the logarithmic term at first order is not significant. In

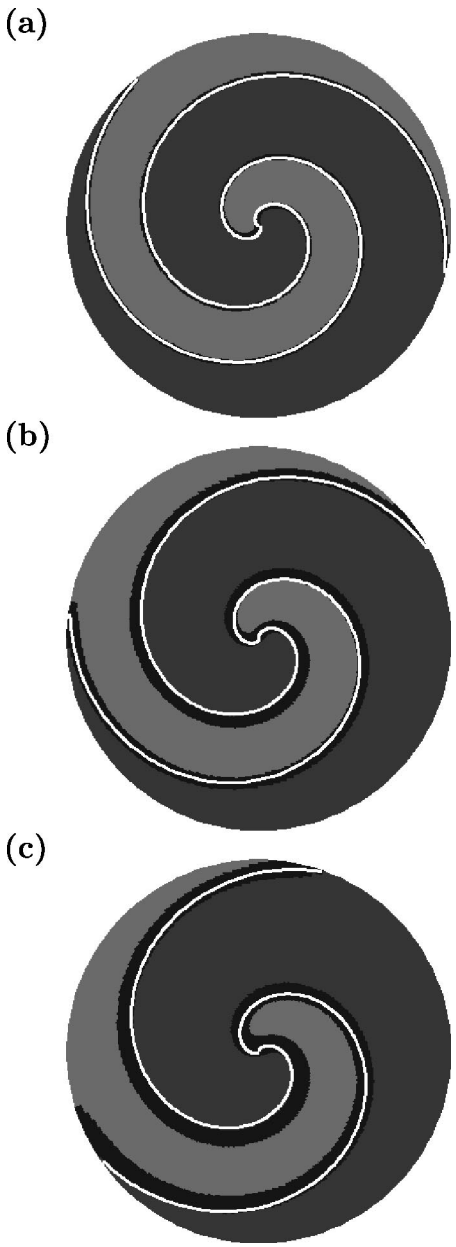

FIG. 7. Comparison between spiral solutions from reaction–diffusion equations and shapes obtained from asymptotics using Recipe 2. The u-field from Eqs. (3) is shown with excited ($u>0.9$), quiescent ($u<0.1$), and interfaces regions ($0.1\leqslant u\leqslant 0.9$). (a) $\varepsilon=0.1$, (b) $\varepsilon=0.2$, and (c) $\varepsilon=0.27144$. Other parameters are $a=1.0$, $b=0.1$ and the domain radius is 20.

the spirit of keeping the recipes simple while not unnecessarily sacrificing accuracy, we do not include this term.

Note that the relative chirality of the spirals in Figs. 5 and 6 is significant. The first-order correction reduces the pitch of the leading order spiral.

Now we consider how the spiral shapes from asymptotics, $\Phi^{+}(r)$ and $\Phi^{-}(r)$, compare with full solutions of reaction–diffusion equations (3). The comparison is shown in Figs. 7 and 8 for fixed values of a and b. In Fig. 7 we present comparisons for the three values of ε considered in Fig. 3. Apart from choosing the phase Φ_0 in Recipe 2, there are no adjustable parameters. At first order, the asymptotic results capture very well the spiral shapes. By contrast, the

FIG. 8. Comparison between spiral solutions from reaction–diffusion equations with $\varepsilon=0.2$ and shapes obtained from leading-order asymptotics, Recipe 1. All parameters are as in Fig. 7(b).

leading-order asymptotics shown in Fig. 8 does not capture quantitatively the spiral shape. Note that the pitch of the leading-order asymptotic shape in Fig. 8 is larger than that of the full solution; the first-order terms reduce the spiral pitch.

In general we find the shape predictions from the asymptotics are not as accurate as the frequency predictions. This is so despite the generally good agreement between asymptotics and full reaction–diffusion solutions seen in Fig. 7. A quantitative example is given in the next section. The reason why the frequency predictions are better than the shape prediction is not clear to us. It may be simply that the higher-order terms are more important for describing the spiral shape than spiral frequency. The shape functions obtained as solutions of the leading- and first-order universal equations have been verified directly against solutions extracted from the full reaction–diffusion equations,[20] so for small ε there is no question of the accuracy of the asymptotic results. We note that Keener[30] has considered a correction to the leading-order asymptotics which involves careful examination of the core. If one looks at those results one also finds that the frequency correction is more accurate than the shape correction.

C. Dispersion curves

We conclude our treatment of spiral waves by considering briefly an important application of the asymptotic results. From the asymptotic recipes it is possible to derive the dispersion relation for spiral waves. This is $\omega(k)$, the relationship between spiral frequency and spiral pitch or wave number k. There are many equivalent ways to express this relationship, e.g., wave speed as a function of wavelength $c(\lambda=2\pi/k)$, frequency as a function of wavelength $\omega(\lambda)$, etc. (see, e.g., Refs. 6, 25, and 31).

In Fig. 9 we show the dispersion relation as $\omega(k)$ for spirals with a in the range $0.5\leqslant a\leqslant 1.2$ with $b=0.1$ and $\varepsilon=0.2$. (Note that this is not the dispersion curve for a planar wave at fixed parameter values.) The points are from full reaction–diffusion solutions where we have extracted the spiral pitch k from the solutions (e.g., Fig. 7) by fitting the interfaces to Archimedean curves $\phi=kr$ for $r>10$. The solid curve is the asymptotic prediction at first order, where

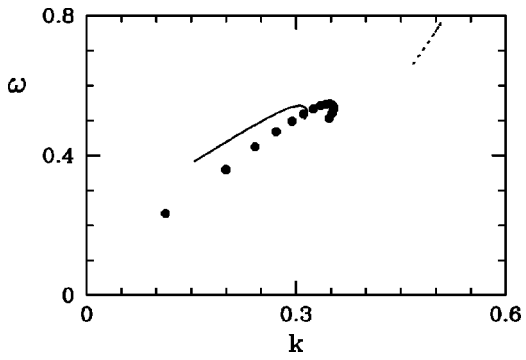

FIG. 9. Dispersion relation for spirals with a from 0.5 to 1.2 with $b=0.1$ and $\varepsilon=0.2$. Asymptotics to first order are shown as solid curve; leading order asymptotics are shown as dashed. Points are from solutions to the reaction–diffusion equations.

$k=k^{(0)}+\varepsilon k^{(1)}$. For comparison we also show the leading-order dispersion curve $\omega^{(0)}(k^{(0)})$. It is again seen that at first order the asymptotics is in reasonable quantitative agreement with full solutions to the reaction–diffusion equations. The difference between the asymptotics and the full solutions is primarily due to inaccuracy in the asymptotic prediction for wave number k; the frequency is quite accurate except for a near 0.5 (the smaller values of ω in Fig. 9). This property of the asymptotics has been noted at the end of Sec. IV B.

V. RECIPES FOR SCROLL WAVES

Here we extend the asymptotic results to the case of twisted scroll waves with straight filaments. Figure 10 shows such a wave. We work in cylindrical coordinates (r,ϕ,z) in which the scroll filament, or axis of rotation, is the z axis.

Solutions to the reaction–diffusion equations are again described by two interfaces dividing the medium into excited and quiescent regions. In this case the interfaces are surfaces parametrized by two parameters. We may take these to be the coordinates r and z, and we denoted the surfaces by $\Phi_2^{\pm}(r,z)$. Points on the wave back satisfy $(r,\phi,z)=(r,\Phi_2^{-}(r,z),z)$ and similarly for the wave front.

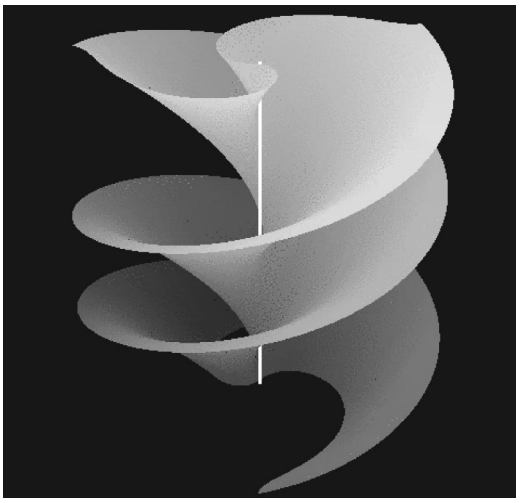

FIG. 10. Twisted scroll wave from numerical solutions of Eqs. (3). The isosurface $u=0.5$ is shown. The scroll filament is white. The universal twist (defined in the text) is $\tilde{\tau}_w=0.4$ corresponding to a twist of $\tau_w\approx 0.35$. Parameters are $a=1.0$, $b=0.1$, $\varepsilon=0.2$.

Twist refers to the rate of change in polar angle of the interface with distance along the interface.[32,33] Commonly in excitable media this is denoted by w but to avoid confusion with the frequency ω we shall use τ_w to denote the scroll twist. We consider the case of constant twist such that $\tau_w=d\Phi_2^{\pm}/dz$ is the same everywhere on the scroll surface. For such waves, the description of the scroll surface in three dimensions reduces to

$$\Phi_2^{\pm}(r,z)=\Phi^{\pm}(r)+\tau_w z, \tag{28}$$

where $\Phi^{\pm}(r)=\Phi_2^{\pm}(r,0)$. Thus we are able to describe the solutions entirely with curves in the plane: $\Phi^{\pm}(r)$. The solutions are understood to be parametrized by the twist τ_w, and we can seek solutions for any τ_w. For $\tau_w=0$ we recover the case of spiral waves.

Only minor changes are required to take into account the effect of twist. We stress only the differences with the previous case of spiral waves.

A. Leading order universal equation

The result of the matched asymptotic analysis at leading order is as follows.[9,20] The wave front and wave back have identical shape with constant angular separation between the two. This separation is independent of the twist and thus the same as for spiral waves, Eq. (6).

The leading-order universal equation with twist is

$$q\frac{d\Psi^{(0)}}{d\tilde{r}}+\frac{\Psi^{(0)}(1+\Psi^{(0)2})}{\tilde{r}}=\tilde{r}(q+\Psi^{(0)2})-B(q+\Psi^{(0)2})^{3/2}, \tag{29}$$

where

$$q\equiv 1+\tilde{\tau}_w^2\tilde{r}^2, \tag{30}$$

$$\tilde{\tau}_w\equiv \tau_w/\sqrt{\omega^{(0)}}, \tag{31}$$

and $\Psi^{(0)}$ and $\tilde{r}$ have the same definitions as in the case of spiral waves, Eqs. (8) and (9). B is again related to the rotation frequency by the relation

$$B=(\mu/\omega^{(0)})^{3/2}, \tag{32}$$

where μ is model dependent and is given by Eq. (14) for Eqs. (2). $\Psi^{(0)}$ and B depend on twist. Hence $\omega^{(0)}$, and all quantities depending on $\omega^{(0)}$ such as $\tilde{r}$, depend on twist.

The boundary condition at $\tilde{r}=0$ is again

$$\Psi^{(0)}(\tilde{r}=0)=0.$$

The large-$\tilde{r}$ behavior of $\Psi^{(0)}$ from Eq. (29) is

$$\Psi^{(0)}(\tilde{r}\to\infty)=-\frac{\tilde{r}}{B}\sqrt{1-\tilde{\tau}_w^2B^2}-\frac{1}{B^2}+O\left(\frac{1}{\tilde{r}}\right). \tag{33}$$

1. Comments

The selection mechanism at leading order is the same as for spiral waves at leading order: the universal equation will have a solution with the required boundary condition and large-$\tilde{r}$ behavior only for a specific (selected) value of B. This selects the scroll rotation frequency $\omega^{(0)}$ via Eq. (32).

The solution $\Psi^{(0)}(\tilde{r})$ to the universal equation then captures the scroll shape in universal length units. Using $\omega^{(0)}$ the shape $\Phi^{(0)}(r)$ in Fife units can be recovered.

There is an added complication in the case of twisted scrolls which is not present for spiral waves. Just as the appropriate radial coordinate for the universal equation is $\tilde{r}$ (see Sec. III B 1), so too the appropriate universal representation for the twist is $\tilde{\tau}_w$ given by Eq. (31). However, the conversion factor $\sqrt{\omega^{(0)}}$ between universal twist and twist in Fife units depends itself on twist. Thus, until the universal equation is solved, the twist τ_w in Fife units corresponding to any particular value of the universal twist $\tilde{\tau}_w$ is not known. For example, suppose one solves the universal equation for universal twist $\tilde{\tau}_w = 0.4$. Only after the equation is solved will the corresponding value of twist τ_w in Fife units be known. Moreover, the value of τ_w will depend on model parameters—for $a = 1.0$ $b = 0.1$, the value of τ_w is about 0.35 (see Fig. 10), but for other values of a and b the value of τ_w corresponding to $\tilde{\tau}_w = 0.4$ will be different. Stated the other way around, from a practical point of view one wants to choose model parameters and a value of twist in Fife (or other) units, and to then find the shape and frequency of the corresponding scroll wave. One cannot do this directly because one does not know how to convert the twist τ_w to universal twist $\tilde{\tau}_w$ until the universal equation is solved.

A simple way to untangle this is as follows. First note that from Eqs. (31) and (32),

$$\frac{\tau_w^2}{\mu} = \frac{\tilde{\tau}_w^2}{B^{2/3}}.$$

On the right-hand side appears only universal quantities—quantities appearing in the universal equation. The left-hand side must therefore also be universal. The left-hand side can, however, be computed directly from the twist τ_w and model parameters. Thus universal solutions can be readily used if given in terms of $\tilde{\tau}_w^2/B^{2/3}$ rather than $\tilde{\tau}_w$.

The important quantity is B because from this the frequency is given and the shape can be well approximated by the large-$\tilde{r}$ expression, Eq. (33). Figure 11(a) shows B as a function of τ_w^2/μ from solutions to the universal equation. These data have been obtained by numerically solving the equation for specified values of $\tilde{\tau}_w$. Then from the values of B resulting from the solution, $\tilde{\tau}_w^2/B^{2/3}$ has been found and plotted but labeled by the equivalent, but more useful τ_w^2/μ.

The data in the figure are well approximated by

$$B \simeq B_0 + B_1\left[\frac{\tau_w^2}{\mu}\right] + B_2\left[\frac{\tau_w^2}{\mu}\right]^2 + B_3\left[\frac{\tau_w^2}{\mu}\right]^3, \tag{34}$$

where

$$B_0 = 1.738, \quad B_1 = -1.405, \quad B_2 = 0.936,$$

$$B_3 = -0.277.$$

2. Recipe 3

We now give a simple recipe for obtaining leading-order approximations to straight twisted scroll waves in reaction–diffusion Eqs. (1) or (3).

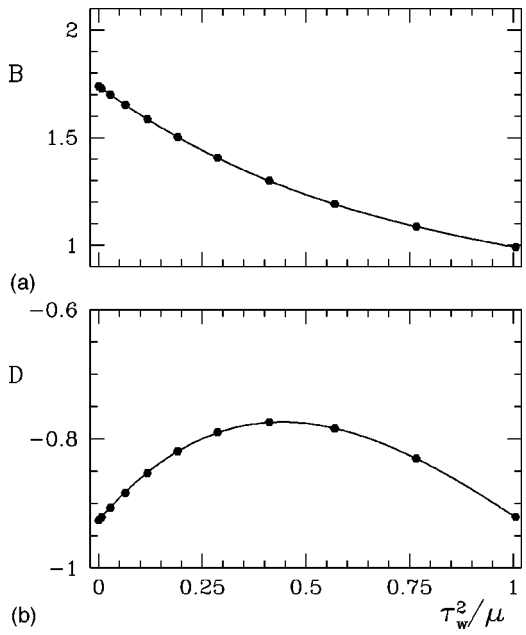

FIG. 11. Dependence of the eigenvalues B and D on twist. Points are from solutions to universal Eqs. (29) and (36). Curves are polynomial approximations, Eqs. (34) and (39).

Use Eqs. (13) and (14) to find μ for desired model parameters a and b. Then for any desired value of twist τ_w, find the value of B via approximation (34). Then with this value of B the leading-order frequency and scroll shape are

$$\omega^{(0)} = \mu/B^{2/3}, \tag{35a}$$

$$\Phi_2^{(0)+}(r,z) = \Phi_0 - k^{(0)}r - \frac{1}{B^2}\ln r + \tau_w z, \tag{35b}$$

$$\Phi_2^{(0)-}(r,z) = \Phi_2^{(0)+}(r,z) - 2\pi v^s, \tag{35c}$$

where

$$k^{(0)} = \frac{\sqrt{\omega^{(0)} - \tau_w^2 B^2}}{B} \tag{35d}$$

with Φ_0 a constant of integration which sets the arbitrary phase of the scroll wave. Comparisons with numerical solutions of the reaction–diffusion equations are given in Sec. V C.

B. First order universal equation

There is no contribution to the separation between wave front and wave back at first order: $\Delta\Phi^{(1)} = 0$ as for spiral waves in Eq. (17). The universal equation for the straight twisted scroll wave is

$$q\frac{d\Psi^{(1)}}{d\tilde{r}} + l(\tilde{r})\Psi^{(1)} = Dm_1(\tilde{r}) + m_2(\tilde{r}), \tag{36}$$

where $\Psi^{(1)}$ and D are defined as in the case of spiral waves, Eqs. (19) and (23), respectively, and q is defined by Eq. (30). Functions $l(\tilde{r})$, $m_1(\tilde{r})$, and $m_2(\tilde{r})$ are given by

$$l(\tilde{r}) = \frac{1}{\tilde{r}} + \tilde{r}\Psi^{(0)} + 3\Psi^{(0)}\left[\frac{\Psi^{(0)}}{\tilde{r}} - \tilde{r} + B\sqrt{q+\Psi^{(0)2}}\right],$$

$$m_1(\tilde{r}) = \tilde{r}(q+\Psi^{(0)2}) + B(q+\Psi^{(0)2})^{3/2},$$

$$m_2(\tilde{r}) = \frac{5}{3}\frac{(q+\Psi^{(0)2})^2}{\tilde{r}}.$$

These depend on twist through q and through the dependence of $\Psi^{(0)}$ on twist.

The large-$\tilde{r}$ behavior of $\Psi^{(1)}$ from Eq. (36) is

$$\Psi^{(1)}(\tilde{r}\to\infty) = -\frac{6DB^2+5}{3B^3}\frac{\tilde{r}}{\sqrt{1-\tilde{\tau}_w^2 B^2}} - \frac{3DB^2+5}{B^4} + O\left(\frac{1}{\tilde{r}}\right).$$

The solution to the universal equation can be found in principle by integration. The solution is

$$\Psi^{(1)}(\tilde{r}) = \Psi_h^{(1)}(\tilde{r})\int_0^{\tilde{r}} \frac{Dm_1(\rho)+m_2(\rho)}{\Psi_h^{(1)}(\rho)}d\rho, \tag{37}$$

where Ψ_h is the solution to the homogeneous problem given by

$$\Psi_h^{(1)} = \frac{1}{q\tilde{r}}(q+\Psi^{(0)2})^{3/2}\exp\left(-\int_0^{\tilde{r}}\frac{\rho\Psi^{(0)}(\rho)}{1+\tilde{\tau}_w^2\rho^2}d\rho\right). \tag{38}$$

1. Comments

The selection mechanism at first order is the same as for spiral waves at this order: the first order shape function $\Psi^{(1)}(\tilde{r})$ given by Eq. (37) will diverge exponentially unless D has the selected value

$$D = -\frac{c_2}{c_1},$$

where

$$c_i = \int_0^\infty [m_i(\rho)/\Psi_h^{(1)}(\rho)]d\rho.$$

The value of D now depends on twist. Figure 11(b) shows D as a function of τ_w^2/μ from numerical solutions to the universal equation at first order. The values are well approximated by the following:

$$D \simeq D_0 + D_1\left[\frac{\tau_w^2}{\mu}\right] + D_2\left[\frac{\tau_w^2}{\mu}\right]^2 + D_3\left[\frac{\tau_w^2}{\mu}\right]^3, \tag{39}$$

where

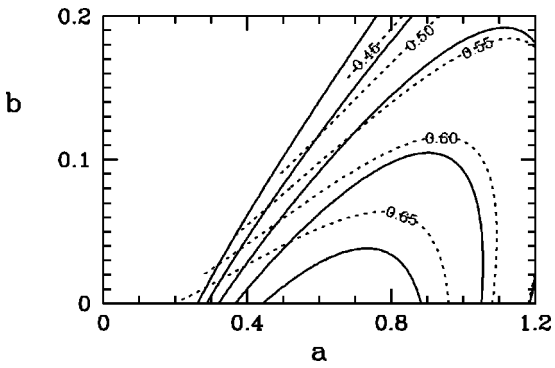

FIG. 12. Comparison of frequency ω from asymptotics at first order (solid) and full solutions of reaction–diffusion equations (dashed) for $\varepsilon = 0.2$ and a fixed value of $\tilde{\tau}_w = 0.4$. The contour levels for the reaction–diffusion equations (labeled) are the same as for the asymptotics (not labeled).

$$D_0 = -0.926, \quad D_1 = 0.748, \quad D_2 = -1.052, \quad D_3 = 0.311.$$

2. Recipe 4

Finally we give a recipe for obtaining leading-plus-first order approximations to scroll waves in Eqs. (1) or Eqs. (3). First use Recipe 3 to obtain $\omega^{(0)}$ and $\Phi_2^{(0)\pm}$. Use Eq. (39) to find D for the relevant values of twist and model parameters. Then calculate

$$\omega^{(1)} = D/a, \tag{40a}$$

$$\Phi^{(1)+}(r) = -k^{(1)}r, \tag{40b}$$

where

$$k^{(1)} = \frac{6DB^2+5}{3aB^3\sqrt{\omega^{(0)}-\tau_w^2B^2}}.$$

Then

$$\omega = \omega^{(0)} + \varepsilon\omega^{(1)}, \tag{41a}$$

$$\Phi_2^+(r,z) = \Phi_2^{(0)+}(r,z) + \varepsilon\Phi^{(1)+}(r), \tag{41b}$$

$$\Phi_2^-(r,z) = \Phi_2^+(r,z) - 2\pi v^s. \tag{41c}$$

This final recipe gives the scroll frequency and shape as a function of twist and all three parameters a, b, and ε appearing in the reaction–diffusion equations.

C. Comparison for scroll waves

We present here a brief comparison between asymptotic predictions and full solutions of the reaction–diffusion equations for the case of twisted straight scroll waves. Figure 12 shows a frequency comparison throughout the a–b parameter plane for fixed ε and $\tilde{\tau}_w$, while Fig. 13 compares the shape of a particular twisted scroll with the asymptotic shape. The scrolls displayed in Figs. 10 and 13 are the same. Figure 13 shows the u concentration at a fixed z location; all other z locations are equivalent apart from the rotation in ϕ seen in Fig. 10.

The twist chosen for the scroll in Figs. 10 and 13 correspond to about the upper limit of twist that would normally

FIG. 13. Comparison between twisted-scroll solutions from reaction–diffusion equations and shapes obtained from asymptotics using Recipe 4. Quantities are shown at a fixed z location. The u field from Eqs. (3) is shown with excited ($u>0.9$), quiescent ($u<0.1$), and interfaces regions ($0.1\leqslant u\leqslant 0.9$). Parameters are $a=1.0$, $b=0.1$, $\varepsilon=0.2$, and the domain radius is 20. $\tilde{\tau}_w=0.4$ corresponding to $\tau_w\approx 0.35$ for these value of a and b.

be of interest; the twist just slightly exceeds the value giving rise to instability at parameter values in the caption.[20]

From Figs. 12 and 13 it can be seen that the asymptotic predictions are good and moreover that there is little qualitative difference between these cases and those for spiral waves at the same value of ε. See specifically Figs. 3 and 7 for $\varepsilon=0.2$.

VI. FILAMENT DYNAMICS

It is possible to use the asymptotic results to derive explicitly coefficients in the laws for scroll filament dynamics.[34–37] In short, the theory of filament dynamics attempts to describe the behavior of scroll waves in terms of the motion of scroll filaments and the rotation of waves about these filaments. The theory is derived for the case of scroll waves weakly perturbed from straight, untwisted scrolls. The successes and shortcomings of this theory are treated elsewhere.[36–38]

What interests us here is that one of the three equations in the theory describes the change in local scroll rotation frequency due to twist. This equation is

$$\omega=\omega_0-a_1\tau_w^2+b_1 d\tau_w/ds, \tag{42}$$

where ω_0 is the frequency of the straight untwisted scroll, i.e., the spiral frequency, a_1 and b_1 are coefficients depending on the medium, and $d\tau_w/ds$ is the rate of change of twist along the filament. This last term is zero when the twist is uniform. There are two equations in the theory describing the motion of the scroll filament in normal and binormal directions for curved filaments. We discuss these effects briefly below.

In the derivation of Eq. (42), a two-dimensional spiral wave with frequency ω_0 is assumed to exist, and the twist and its derivative τ_w and $d\tau_w/ds$ are taken to be small. No assumption is made on ε in the reaction–diffusion equations. While formulas exist for the coefficients a_1 and b_1, these formulas require the adjoint eigenfunctions of a linear operator defined in terms of the spiral solution. Hence they have never been used to obtain a_1 and b_1.

In contrast, the approach we have taken is to consider the asymptotics of small ε and to focus on the case of uniform twist: $d\tau_w/ds=0$. As a result, we are able to obtain explicitly ω_0 and a_1 as expansions in ε. Furthermore, we are not restricted in the size of τ_w we can consider. In principle we can obtain higher-order (in τ_w) corrections to Eq. (42).

Using the recipes in this paper we obtain

$$\omega=\omega_0-a_1\tau_w^2+O(\tau_w^4), \tag{43}$$

where

$$\omega_0=0.692\mu-\varepsilon\frac{0.926}{a}+O(\varepsilon^2), \tag{44}$$

$$a_1=-0.373-\varepsilon\frac{0.748}{a\mu}+O(\varepsilon^2). \tag{45}$$

The numerical factors have been obtained from B_0, B_1, D_0, and D_1. Equations (43)–(45) provides simple expressions for ω_0 and a_1 to two orders in ε. Based on the comparisons already shown in this paper, they should be reasonably accurate over a large range of model parameters (a, b, ϵ) and for moderate values of twist, including most cases of practical interest. For example, for the scroll shown in Figs. 10 and 13 the frequency given by Eqs. (43)–(45) is $\omega=0.600$, whereas the frequency from the full solution of the reaction–diffusion equations is $\omega=0.608$. If needed, one can obtain the corrections at higher powers of τ_w in Eq. (43) from the constants B_0, etc., already given. For other attempts to estimate theoretically and measure numerically a_1 see Refs. 36 and 39.

Finally, we consider briefly the other equations in the theory of filament dynamics. There are two equations governing filament motion in the normal and binormal directions. Taking into account symmetries, these equations are[35]

$$V_n=b_2\kappa,$$

$$V_b=c_3\kappa,$$

where V_n and V_b are the local velocities of the filament in the normal and binormal directions, κ is the local filament curvature and b_2 and c_3 are coefficients which depend on the medium. These coefficients are analogous to a_1 and b_1 appearing in Eq. (42). As with those coefficients, the formulas for b_2 and c_3 require the adjoint eigenfunction of an operator defined in terms of the spiral solution, and thus these coefficients have never been computed analytically.

At the current time only the leading-order asymptotics is complete for the general case of a curved, twisted filament. At this order the asymptotics predicts that b_2 and c_3 vanish, that is that the filament motion vanishes as $\varepsilon\to 0$.

We illustrate this in Fig. 14 where we show b_2 as a function of ε. In this case the value of b_2 has been obtained by numerically simulating the collapse of axisymmetric scroll rings (see Refs. 39 and 40). The normal velocity of the ring is indeed found to be proportional to curvature and the proportionality gives the value of b_2. This value goes to zero as a function of ε as expected from the leading-order asymptotics. The binormal velocity can also be found, but it is significantly smaller (in this case) and the values of c_3 are much more uncertain than those for b_2.

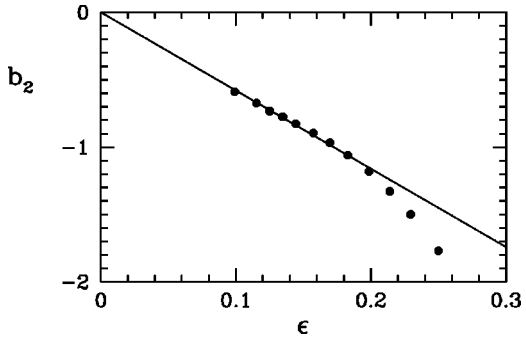

FIG. 14. Normal-velocity coefficient b_2 as a function of ε for fixed model parameters $a=1.0$ and $b=0.1$. The line is drawn to show the regime where b_2 is well approximated by $\varepsilon b_2^{(1)}$.

What is intriguing here is that there is a large regime for which $b_2 \approx \varepsilon b_2^{(1)}$ for some as yet analytically unknown value of $b_2^{(1)}$. It can be found numerically for particular parameter values such as those considered in Fig. 14, but it is not known in general.

This illustrates the power of the asymptotic approach we have pursued. While there seems little hope of obtaining the values of b_2 and c_3 using the expressions given in Refs. 34 and 35, there clearly is some hope of finding analytical formulas for the first-order contribution $b_2^{(1)}$ and $c_3^{(1)}$. This would be a major achievement as it would give explicitly the equations of filament motion for a considerable range of parameter values.

VII. SUMMARY

In this paper we have given simple recipes for obtaining the frequencies and shapes of waves in a model of excitable media. The recipes apply to spiral waves and to scroll waves with straight filament and uniform twist. They are based on asymptotic universal equations at leading and first order in the asymptotic parameter ε. The recipes are specifically designed to be used without further need for solving these differential equations. We have presented numerous comparisons between the predictions of the asymptotic recipes and full solutions of the reaction–diffusion model, and in so doing we have demonstrated the range of validity for these predictions. Finally, we have discussed the connection between the asymptotic results and the equations of filament dynamics. Specifically we have evaluated one of the previously unknown coefficients in this theory and we have discussed the promise for progress in this direction.

There are many directions this work could go in the future. One direction that probably should not be pursued is the $O(\varepsilon^2)$ correction to the formulas given here. The reason for this can be seen in Fig. 1(c). While not all of our numerical computations show such excellent agreement with the first-order asymptotics, we have never seen a case for which the next-order correction would appear to offer significant improvement. The qualitatively important effect not captured by the first-order asymptotics is the frequency drop as the system approaches the point of wave propagation failure (see Sec. V A). This is not an $O(\varepsilon^2)$ effect. What would be very valuable is to use, and probably extend, the work of Hakim and Karma[19] on the asymptotics at the point of propagation failure to obtain a complete asymptotic description of waves throughout parameter space.

Because the asymptotic predictions for the frequency of spiral and twisted scroll waves are particularly simple, and because the frequency is a particularly important quantity, we conclude with a summary of these predictions. Equations (43)–(45) together with Eqs. (13) and (14) give the frequency of scroll solutions to Eqs. (3). The units are Fife units. Since Eqs. (1) with $D_n=1$ have been considered often in the literature, it is worthwhile recasting these formulas in the units of these equations. We have

$$\omega_n = \omega_{0_n} - a_1 \tau_{wn}^2 + O(\tau_{wn}^4),$$

where

$$\omega_{0_n} = \frac{0.692\mu}{\varepsilon_n^{1/3}} - \frac{0.926}{a} + O(\varepsilon_n^{1/3}),$$

$$a_1 = -0.373 - \frac{0.748\varepsilon_n^{1/3}}{a\mu} + O(\varepsilon_n^{2/3})$$

with

$$\mu \simeq 2.70\left[\frac{v^s(1-v^s)}{a}\right]^{2/3}, \quad v^s = \frac{a}{2} - b.$$

For small and even not so small values of ε_n, these remarkably simple formulas give the frequency of solutions of Eqs. (1) and (2) as a function of all three model parameters, a, b, and ε_n, and as a function of twist τ_{w_n} measured in the length units of Eqs. (1) and (2). For zero twist they simplify even further giving the frequency of spiral waves.

ACKNOWLEDGMENTS

This paper originated in part from a series of email exchanges with Art Winfree concerning the asymptotic results and the meaning of the Fife limit and we thank him for his helpful comments and suggestions. We also thank Laurette Tuckerman for her suggestions. D.B. wishes to thank the CNRS and the Laboratoire d'Informatique pour la Mécanique et les Sciences de l'Ingénieur where parts of the work were conducted.

APPENDIX A: COMPUTING FIRST-ORDER UNIVERSAL FUNCTION

Here we describe a computational procedure for obtaining the first-order universal function. This function is given by

$$\Psi^{(1)}(\tilde{r}) = \Psi_h^{(1)}(\tilde{r}) \int_0^{\tilde{r}} \frac{m(\rho)}{\Psi_h^{(1)}(\rho)} d\rho, \tag{A1}$$

where $m(\rho) = Dm_1(\rho) + m_2(\rho)$ and $\Psi_h^{(1)}(\rho)$ is the homogeneous solution. See Secs. III C and V B.

For values of $\tilde{r}$ between 0 and approximately 1, $\Psi^{(1)}(\tilde{r})$ can be found accurately by evaluating the integral using standard methods such as the trapezoidal rule. This procedure gives an inaccurate evaluation of $\Psi^{(1)}(\tilde{r})$ for larger values of $\tilde{r}$ because of the exponential behavior of $\Psi_h^{(1)}(\rho)$.

For values of $\tilde{r}$ larger than order one we obtain $\Psi^{(1)}(\tilde{r})$ as follows. First, Eq. (A1) is rewritten as

$$\Psi^{(1)}(\tilde{r}) = \Psi_h^{(1)}(\tilde{r}) \int_\infty^{\tilde{r}} \frac{m(\rho)}{\Psi_h^{(1)}(\rho)} d\rho,$$

where we have used $\int_0^\infty m(\tilde{r})/\Psi_h^{(1)}(\rho)d\rho = 0$. Then we transform the integral by letting $x = 1 - \tilde{r}/\rho$:

$$\Psi^{(1)}(\tilde{r}) = -\tilde{r} \int_0^1 \frac{m\left(\frac{\tilde{r}}{(1-x)}\right)}{(1-x)^2} \frac{\Psi_h^{(1)}(\tilde{r})}{\Psi_h^{(1)}\left(\frac{\tilde{r}}{(1-x)}\right)} dx.$$

This is more suitable form for finding $\Psi^{(1)}$ when $\tilde{r}$ is of order one and larger. The integrand is small everywhere except in a small neighborhood of $x = 0$ (corresponding to $\rho = \infty$).

To deal with the singularity at $x = 0$ we separate off the integral over the boundary layer near $x = 0$ and introduce stretched coordinates in this region. Let $\tilde{r} = 1/\delta$, choose η such that $\delta^3 \ll \eta \ll 1$ and split this integral into two parts: one from 0 to η and the other from η to 1. For the first integral introduce the stretched coordinate $\overline{x} = x/\delta^3$. This gives

$$\begin{aligned}\Psi^{(1)}(\tilde{r} = 1/\delta) = &-\delta^2 \int_0^{\eta/\delta^3} \frac{m(1/\delta(1-\delta^3\overline{x}))}{(1-\delta^3\overline{x})^2} \\ &\times \frac{\Psi_h^{(1)}(1/\delta)}{\Psi_h^{(1)}(1/\delta(1-\delta^3\overline{x}))} d\overline{x} \\ &- \frac{1}{\delta} \int_\eta^1 \frac{m(1/\delta(1-x))}{(1-x)^2} \frac{\Psi_h^{(1)}(1/\delta)}{\Psi_h^{(1)}(1/\delta(1-x))} dx. \end{aligned} \tag{A2}$$

A suitable choice for η is $\eta = \delta^2$.

Thus for $\tilde{r}$ of order 1 and smaller we find $\Psi^{(1)}(\tilde{r})$ using Eq. (A1) and for $\tilde{r}$ of order 1 and larger we find $\Psi^{(1)}(\tilde{r})$ using Eq. (A2). In both cases we evaluate the integrals using the trapezoidal method.

The universal value D is found in this same way except that rather than using m in the integrand, we used separately m_1 and m_2.

APPENDIX B: FITZHUGH–NAGUMO MODEL

Because the recipes given in the paper are obtained from universal equations, they can be applied directly to a large class of models. As an example we consider here the Fitzhugh–Nagumo model given by the following kinetic functions:

$$f(u,v) = 3u - u^3 - v, \quad g(u,v) = u - \delta.$$

To obtain predictions of the rotation frequencies from the recipes, all we require are the (model dependent) relationships between the universal eigenvalues B and D, and the frequencies $\omega^{(0)}$ and $\omega^{(1)}$. The leading order recipes (Recipe 1 and Recipe 3) are unchanged with the exception that μ is not obtained from Eqs. (13)–(14) but as[12]

$$\mu^{3/2} = \pi(3 - \delta^2)/\sqrt{24}.$$

At first order the only required change in the recipes is that rather than Eqs. (26a) and (40a) we have

$$\omega^{(1)} = D/2.$$

Then in the units of Eqs. (1) with $D_n = 1$, the predicted frequency for spiral and twisted scroll waves in the Fitzhugh–Nagumo model is

$$\omega_n = \omega_{0_n} - a_1 \tau_{wn}^2,$$

where

$$\omega_{0_n} = \frac{0.692\mu}{\varepsilon_n^{1/3}} - 0.463, \quad a_1 = -0.373\left(1 + \frac{\varepsilon_n^{1/3}}{\mu}\right),$$

with μ given by

$$\mu = 0.744(3 - \delta^2)^{2/3}.$$

(We have used $0.373 \simeq 0.748/2$.)

[1] A. T. Winfree, *When Time Breaks Down* (Princeton University Press, Princeton, NJ, 1987).
[2] *Chemical Waves and Patterns*, edited by R. Kapral and K. Showalter (Kluwer, London, 1995).
[3] P. C. Fife, in *Non-Equilibrium Dynamics in Chemical Systems*, edited by C. Vidal and A. Pacault (Springer-Verlag, Berlin, 1984), pp. 76–88.
[4] P. C. Fife, J. Stat. Phys. **39**, 687 (1985).
[5] J. P. Keener and J. J. Tyson, Physica D **21**, 307 (1986).
[6] J. J. Tyson and J. P. Keener, Physica D **32**, 327 (1988).
[7] E. Meron and P. Pelce, Phys. Rev. Lett. **60**, 1880 (1988).
[8] D. Kessler and H. Levine, Physica D **39**, 1 (1989).
[9] A. Bernoff, Physica D **53**, 125 (1991).
[10] P. Pelce and J. Sun, Physica D **48**, 353 (1991).
[11] A. S. Mikhailov and V. S. Zykov, Physica D **52**, 379 (1991).
[12] A. Karma, Phys. Rev. Lett. **68**, 397 (1992).
[13] D. Kessler, H. Levine, and W. Reynolds, Phys. Rev. Lett. **68**, 401 (1992).
[14] E. Meron, Phys. Rep. **218**, 1 (1992).
[15] A. S. Mikhailov, V. A. Davydov, and V. S. Zykov, Physica D **70**, 1 (1994).
[16] D. Kessler and R. Kupferman, Physica D **97**, 509 (1996).
[17] D. Kessler and R. Kupferman, Physica D **105**, 207 (1997).
[18] V. Hakim and A. Karma, Phys. Rev. Lett. **79**, 665 (1997).
[19] V. Hakim and A. Karma, Phys. Rev. E **60**, 5073 (1999).
[20] D. Margerit and D. Barkley, Phys. Rev. Lett. **86**, 175 (2001).
[21] D. A. Kessler, J. Koplik, and H. Levine, Adv. Phys. **37**, 255 (1988).
[22] D. Barkley, Physica D **49**, 61 (1991).
[23] M. Dowle, R. M. Mantel, and D. Barkley, Int. J. Bifurcation Chaos Appl. Sci. Eng. **7**, 2529 (1997).
[24] D. Barkley, M. Kness, and L. S. Tuckerman, Phys. Rev. A **42**, 2489 (1990).
[25] A. T. Winfree, Chaos **1**, 303 (1991).
[26] D. Barkley, Phys. Rev. Lett. **68**, 2090 (1992).
[27] D. Barkley, in *Chemical Waves and Patterns*, edited by R. Kapral and K. Showalter (Kluwer, Dordrecht, 1995), pp. 163–190.
[28] A. Karma, Phys. Rev. Lett. **66**, 2274 (1991).
[29] D. Barkley, Phys. Rev. Lett. **72**, 164 (1994).
[30] J. P. Keener, SIAM (Soc. Ind. Appl. Math.) J. Appl. Math. **52**, 1370 (1992).
[31] A. L. Belmonte, Q. Quyang, and J.-M. Flesselles, J. Phys. II **7**, 1425 (1997).
[32] A. T. Winfree and S. H. Strogatz, Physica D **9**, 65 (1983).
[33] J. J. Tyson and S. H. Strogatz, Int. J. Bifurcation Chaos Appl. Sci. Eng. **1**, 723 (1991).
[34] J. P. Keener, Physica D **31**, 269 (1988).
[35] V. N. Biktashev, A. V. Holden, and H. Zhang, Philos. Trans. R. Soc. London, Ser. A **347**, 611 (1994).
[36] A. T. Winfree, in *Chemical Waves and Patterns*, edited by R. Kapral and K. Showalter (Kluwer, Dordrecht, 1995), pp. 3–55.
[37] A. T. Winfree, SIAM Rev. **32**, 1 (1990).
[38] J. J. Tyson and J. P. Keener, in *Chemical Waves and Patterns*, edited by R. Kapral and K. Showalter (Kluwer, Dordrecht, 1995), pp. 93–118.
[39] C. Henze, E. Lugosi, and A. Winfree, Can. J. Phys. **68**, 683 (1990).
[40] M. Courtemanche, W. Skaggs, and A. T. Winfree, Physica D **41**, 173 (1990).